TECHNICAL MEMORANDUM

649

A new prognostic bulk microphysics scheme for the IFS

Richard M. Forbes[1], Adrian M. Tompkins[2] and Agathe Untch[1]

Research Department

[1]ECMWF [2]ICTP, Italy

September 2011

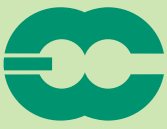

European Centre for Medium-Range Weather Forecasts
Europäisches Zentrum für mittelfristige Wettervorhersage
Centre européen pour les prévisions météorologiques à moyen terme

Series: ECMWF Technical Memoranda

A full list of ECMWF Publications can be found on our web site under:
http://www.ecmwf.int/publications/

Contact: library@ecmwf.int

European Centre for Medium-Range Weather Forecasts
Shinfield Park, Reading, RG2 9AX, England

Abstract

A major upgrade to the parametrization of stratiform cloud and precipitation was implemented in the Integrated Forecast System (IFS) Cycle 36r4, operational at ECMWF from 9 November 2010. Three additional prognostic variables have been introduced to enable a more physically based representation of mixed-phase (liquid/ice) cloud and precipitating rain and snow. A fully implicit method is employed to solve the network of microphysics pathways stably for long timesteps. It is the most significant change to the structure of the cloud parametrization since the Tiedtke scheme was introduced operationally in 1995. Many aspects of the model are systematically improved including the skill of precipitation forecasts, the spatial distribution of ice and snow in the troposphere, the physical processes in mixed-phase cloud and the impact of cloud and precipitation on radiation.

1 Introduction

The Tiedtke cloud scheme, described fully in Tiedtke (1993), has served the Integrated Forecast System (IFS) well since its implementation in 1995. The scheme represents clouds in terms of two prognostics parameters; the first describing the horizontal coverage of the grid box by cloud, and the second representing the mass mixing ratio of total cloud condensate, which is divided into separate liquid and ice categories diagnostically according to temperature. The approach includes parametrizations of the sources and sinks of the prognostic cloud variables due to all the major generation and destruction processes, including convection and microphysics. On the introduction of the new scheme into operations in 1995, the monitoring of total cloud cover relative to SYNOP observations showed a distinct reduction in the error.

The scheme has since been under continual development with many aspects of the scheme changed from the original code, including the numerical formulation and modifications to microphysical source and sink terms. Improvements have been made to the representation of ice cloud microphysics, including the process of ice sedimentation (Jakob, 2000), and a novel parametrization was developed for the subgrid precipitation coverage which improved the representation of precipitation evaporation/sublimation (Jakob and Klein, 2000). Subsequently the numerics were rewritten to treat all cloud processes in parallel. These changes did not improve the vertical resolution sensitivity of the scheme, and thus more recent changes rejected the exact, semi-implicit cloud water and cover equation solvers in favour of a forward-in-time, upstream implicit approach. This introduced a separate treatment of autoconversion of ice crystals to snow, and reverted to using a constant sedimentation velocity for ice crystals to avoid numerical shocks. This was supplemented by a new parametrization to allow ice supersaturated conditions in the cloud-free part of the grid box (Tompkins *et al.*, 2007). The modified Tiedtke cloud scheme, in conjunction with the data assimilation and underlying forecast model system, has performed competitively with other state-of-the-art forecast models for cloud property predictions (Illingworth *et al.*, 2007; Bouniol *et al.*, 2010).

Despite all the above developments, the basic structure of the cloud scheme has remained essentially the same, with one prognostic variable for cloud fraction and one prognostic variable for cloud condensate. With increasing emphasis on cloud and precipitation in NWP and increasing resolution of the IFS model, it was clear that a number of changes were required to enable the continued improvement of the scheme, both now and looking ahead for the future. Particular issues that needed to be addressed included precipitation advection, representation of mixed-phase cloud, numerical implementation and the physical realism of the scheme. These issues are discussed in turn below to provide the motivation for the developments described in this report.

(i) Precipitation advection: Higher horizontal resolution and shorter timesteps mean the original diagnostic assumptions for precipitation become less valid. The diagnostic approach assumes the time taken for precipitation to fall from cloud to ground is small compared to the timestep of the model and that horizontal advection can be neglected on the spatial scale of the model grid resolution. A prognostic representation of precipitation is therefore required as the model resolution and timestep increase, particularly for snow particles which have a lower density and slower terminal fall speed than raindrops.

(ii) Mixed-phase cloud: The diagnostic approach to the mixed phase, which partitions the cloud condensate into liquid and ice according to temperature in the range 0°C to -23°C, means that both ice and supercooled liquid are always present in cloud in this temperature regime and no liquid water is allowed at temperatures colder than -23°C. The reality can be very different. For example in this sub-zero temperature range, emerging convective clouds are often all liquid, established frontal clouds often all ice and thin mid-level cloud often topped with a shallow supercooled liquid water layer with ice particles precipitating out below. Supercooled liquid water is observed down to temperatures of -30°C and colder (Hogan *et al.*, 2007). If the model is to begin to capture these aspects, then an additional degree of freedom is required with separate prognostic variables for liquid and ice condensate.

(iii) Numerical issues: The diagnostic mixed-phase approach also leads to a number of unrealistic numerical artefacts in the formulation of the microphysical processes, leading to a discontinuity in ice supersaturation and autoconversion of ice to snow at the mixed-phase temperature threshold (-23°C) and a lack of sedimentation of ice in the mixed phase. This significantly affects the physical representation and the spatial distribution of ice in the mixed-phase temperature range. In addition, the diagnostic approach assumes a single saturation curve in the mixed phase varying from water saturation at 0°C to ice saturation at -23°C. In reality different microphysical processes respond differently to ice saturation and water saturation, such as the deposition growth of ice crystals at the expense of water drops (the Wegener-Bergeron-Findeisen mechanism).

(iv) Physical realism: The representation of cloud with just two variables leads to a number of simplifications and approximations in the scheme. Additional degrees of freedom allow for a more physically realistic representation of cloud and precipitation microphysics that can be verified with observations.

This document describes the recent developments to the cloud scheme (implemented in IFS Cycle 36r4) that changes from a single prognostic cloud condensate variable to four prognostic variables for cloud liquid, cloud ice, rain and snow (as well as cloud fraction) in order to address some of the issues above. Section 2 describes the new scheme in terms of changes to the numerical framework, to the microphysical processes and to interactions with other parts of the model. Section 3 highlights some of the impacts on aspects of the model performance and Section 4 provides a concluding summary. The Appendices include technical details of the new prognostic field initialization and the diagnostic output that is available.

2 Description of the new prognostic microphysics scheme

2.1 Overview

The new parametrization of stratiform cloud and precipitation increases the number of prognostic variables from two (cloud fraction, cloud condensate) to five (cloud fraction, cloud liquid water, cloud ice, rain and snow). The philosophy of the original Tiedtke scheme is retained with regards to a prognostic cloud fraction and sources and sinks of all cloud variables due to the major generation and destruction

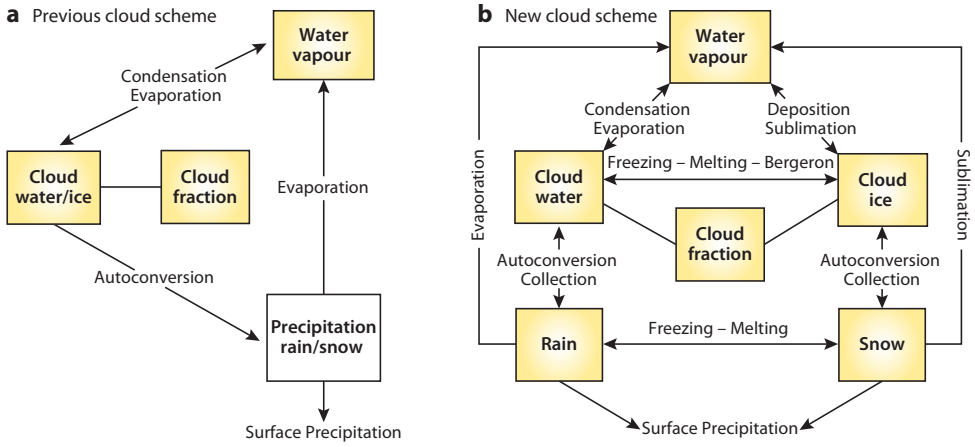

Figure 1: *Schematic of the IFS cloud scheme: (a) the Tiedtke scheme with three moisture related prognostic variables operational from 1995 to 2010 (before IFS Cy36r4) and (b) the new cloud scheme with six moisture related prognostic variables (Cy36r4 onwards). Yellow boxes indicate prognostic variables.*

processes, including detrainment from convection. However, water and ice clouds are now independent, addressing many of the issues identified above and allowing a more physically realistic representation of supercooled liquid water cloud. Rain and snow precipitation are also now able to precipitate with a determined terminal fall speed and can be advected by the three-dimensional wind. A new multi-dimensional implicit solver is implemented for the numerical solution of the cloud and precipitation prognostic equations. Figure 1 shows a schematic to highlight the differences between the new and old parametrization schemes. This section describes the numerical framework and revised microphysical processes in the new scheme. Further details of the cloud and precipitation parametrization scheme can be found in Part 4 of the IFS Documentation for Cycle 37r2 (*www.ecmwf.int/research/ifsdocs/CY37r2*).

2.2 Numerical framework

The new scheme is a multi-species prognostic microphysics scheme, with $m = 5$ prognostic equations for water vapour, cloud liquid water, rain, cloud ice and snow. The equation governing each prognostic cloud variable within the cloud scheme is

$$\frac{\partial q_x}{\partial t} = S_x + \frac{1}{\rho}\frac{\partial}{\partial z}\left(\rho V_x q_x\right), \tag{1}$$

where q_x is the specific water content for category x ($x = 1$ for cloud liquid droplets, $x = 2$ for rain, and so on), S_x is the net source or sink of q_x through microphysical processes, and the last term represents the sedimentation of q_x with fall speed V_x.

The solution to this set of equations uses the upstream approach. Writing the advection term in mass flux form, collecting all fast processes (relative to a GCM timestep) into an implicit term ($\widetilde{B}$) and leaving the rest in an explicit term ($\vec{A}$), gives

$$\frac{q_x^{n+1} - q_x^n}{\Delta t} = A_x + \sum_{y=1}^{m} B_{xy} q_y^{n+1} - \sum_{y=1}^{m} B_{yx} q_x^{n+1} + \frac{\rho_{k-1} V_x q_{x,k-1}^{n+1} - \rho V_x q_x^{n+1}}{\rho \Delta Z}. \tag{2}$$

for timestep n. The subscript "$k-1$" refers to a term calculated at the model level above the present level k for which all other terms are being calculated. The matrix $\widetilde{B}$ (with terms B_{xx}, B_{xy}, B_{yx}) represents all

the implicit microphysical pathways such that $B_{xy} > 0$ represents a source of q_x and a sink of q_y. Matrix $\widetilde{B}$ is positive-definite off the diagonal, with zero diagonal terms since $B_{xx} = 0$ by definition. Some terms, such as the creation of cloud through condensation resulting from adiabatic motion or diabatic heating, are more suitable for an explicit framework, and are retained in the explicit term $\vec{A}$.

Due to the cross-terms q_y^{n+1}, (2) is rearranged to give a straight forward matrix equation which can be solved with standard methods (the scheme currently uses the LU decomposition method). As long as the solution method is robust, the choice for solution is not critical as the number of microphysical prognostic equations is small ($m = 5$), in contrast to chemical models with typically O(100) species. The solution method is simplified by assuming the vertical advection terms due to convective subsidence and sedimentation act only in the downward direction, allowing the solution to be conducted level by level from the model top down. The vertical advection term only appears on the diagonal, thus the matrix equation for a 3-variable system is

$$\begin{pmatrix} 1+\Delta t(\frac{V_1}{\Delta Z}+B_{21}+B_{31}) & -\Delta t B_{12} & -\Delta t B_{13} \\ -\Delta t B_{21} & 1+\Delta t(\frac{V_2}{\Delta Z}+B_{12}+B_{32}) & -\Delta t B_{23} \\ -\Delta t B_{31} & -\Delta t B_{32} & 1+\Delta t(\frac{V_3}{\Delta Z}+B_{13}+B_{23}) \end{pmatrix} \cdot \begin{pmatrix} q_1^{n+1} \\ q_2^{n+1} \\ q_3^{n+1} \end{pmatrix} =$$
$$\left[q_1^n + \Delta t \left(A_1 + \frac{\rho_{k-1} V_1 q_{1,k-1}^{n+1}}{\rho \Delta Z} \right), q_2^n + \Delta t \left(A_2 + \frac{\rho_{k-1} V_2 q_{2,k-1}^{n+1}}{\rho \Delta Z} \right), q_3^n + \Delta t \left(A_3 + \frac{\rho_{k-1} V_3 q_{3,k-1}^{n+1}}{\rho \Delta Z} \right) \right]. \quad (3)$$

There are some aspects that require attention. Firstly, although implicit terms are unable to reduce a cloud category to zero, the explicit can, and often will, achieve this. Thus safety checks are required to ensure that all end-of-timestep variables remain positive definite, in addition to ensuring conservation. Practically, to aid the conservation requirement, the explicit source and sink terms are thus also generalised from a vector $\vec{A}$ to a matrix $\widetilde{A}$, thus

$$\widetilde{A} = \begin{pmatrix} A_{11} & A_{21} & A_{31} \\ A_{12} & A_{22} & A_{32} \\ A_{13} & A_{23} & A_{33} \end{pmatrix}. \quad (4)$$

where $A_{xy} > 0$ represents a source of q_x and a sink of q_y, and $A_{yx} = -A_{xy}$. Although this matrix approach involves a degree of redundancy, it is a simple method of ensuring conservation properties. The matrix diagonals A_{xx} contain the 'external' sources of q_x such as the cloud water detrainment terms from the convection scheme.

In order to simultaneously guarantee conservation and positive-definite properties, the sum of all sinks for a given variable are scaled to avoid negative values. This solution is not accurate, seen from the consideration of the simple case of a variable in equilibrium, with a small initial value subjected to a large source and an equal and opposing sink: the sink will be clipped first and the variable will increase. However, this is deemed preferable to any method that attempts to account for variable sources, which must invoke a sensitivity to the order in which the variables are considered.

The impact on the temperature budget is calculated from the change in cloud variables due to each process after the cloud scheme 'solver' has been applied, and then collecting the terms together that are associated with latent heating/cooling. With the fully implicit solver it is thus easier to use conserved variables to govern the temperature budget; the scheme uses the liquid water temperature T_L defined as:

$$T_L = T - \frac{L_v}{C_p}(q_l + q_r) - \frac{L_s}{C_p}(q_i + q_s). \quad (5)$$

Since $dT_L/dt = 0$, the temperature change is thus given by

$$\frac{\partial T}{\partial t} = \sum_{x=1}^{m} \frac{L(x)}{C_p} \left(\frac{\partial q_x}{\partial t} - D_{q_x} - \frac{1}{\rho} \frac{\partial}{\partial z} (\rho V_x q_x) \right) \tag{6}$$

The first term on the right in the brackets is the rate of change of species q_x due to *all* processes, including the convective detrainment term D_{q_x} and the advective flux terms, which are then subtracted separately since they represent a net T_L flux not associated with latent heating.

For the prognostic cloud fraction variable, denoted by a, there are no multi-dimensional dependencies, so a matrix approach is not required and Eq. 2 simplifies to

$$\frac{a^{n+1} - a^n}{\Delta t} = A + Ba^{n+1}. \tag{7}$$

where A and B are the explicit and implicit source/sink terms for the cloud fraction.

2.3 Revised microphysics

The strategy for the implementation of the prognostic cloud/precipitation variables was to minimize the number of microphysical changes in the existing scheme in order to facilitate the transition to the new framework in the operational model. However, the separation of cloud condensate into liquid and ice prognostic variables clearly requires new microphysical processes to describe the transfer between different water phases in mixed-phase cloud (particularly nucleation and depositional growth of ice crystals). In addition, a number of other alterations to the microphysics are described here.

The numerics previously treated all cloud processes in parallel, but the new scheme treats some processes in a sequential manner. This was necessary to ensure that archived variables made physical sense. For example, if processes are treated contemporaneously, grid boxes could exist with only liquid cloud and no ice at temperatures close to -38°C, since in this approach freshly nucleated liquid cloud droplets must wait until the subsequent timestep before they are able to undergo the freezing process. Thus a first-guess variable is introduced to update the status of variables due to all explicit processes during the course of the scheme.

The formulation of the convective detrainment and subsidence, stratiform condensation and evaporation, and turbulent erosion terms remain essentially the same as in the previous version of the scheme. Each of the new or modified physical process in the cloud scheme is discussed in turn below.

2.3.1 Ice crystal nucleation and ice supersaturation

Ice crystal nucleation is restricted to the homogeneous process, which is parametrized simply, with no attempt made to predict the ice number concentration (N_i) produced by the nucleation event. The ice nucleation occurs on short timescales and is very sensitive to the updraught velocity on the cloud scale, which can only be crudely estimated from GCM resolved variables (Lohmann and Kärcher, 2002; Kärcher and Lohmann, 2002).

To retain consistency with the supersaturation treatment of Tompkins *et al.* (2007), at temperatures below 0°C new cloud forms in any non-cloudy part of the grid box where the humidity exceeds either the minimum of the liquid water saturation specific humidity (q_{sl}), or the critical vapour saturation mixing ratio with respect to ice at which homogeneous ice nucleation initiates (Pruppacher and Klett, 1997;

Koop *et al.*, 2000). For the latter threshold the empirical fit given by Kärcher and Lohmann (2002) is adopted, as before, which is a function of temperature and ranges from 45% supersaturation at $T = 235$ K to 67% at $T = 190$ K:

$$RH_{\text{homo}} = 2.583 - \frac{T}{207.8} \tag{8}$$

where T is the temperature in Kelvin. At temperatures warmer than -38°C the cloud formation over a timestep results entirely in liquid cloud, while below this threshold the liquid water or aqueous sulphate solutes are assumed to freeze instantaneously and the process is a source for cloud ice.

For the case of pure ice cloud formation, the deposition process is considered to be sufficiently rapid relative to the model time-step that it can be approximated by a diagnostic adjustment to exactly ice saturated conditions inside the cloud. This assumption is necessary, since to allow ice supersaturation both within the pure ice cloud and in the clear sky environment would either require a separate prognostic variable to monitor the evolution of the water vapour inside the cloud, or a diagnostic assumption would have to be used to divide the grid-mean humidity between the two regions, which can generate large artificial horizontal sub-grid humidity fluxes (see Tompkins *et al.*, 2007, for more detail). In any case, this assumption appears to be reasonably justified in a wide range of updraught situations by modelling of the homogeneous nucleation process (Khvorostyanov and Sassen, 1998). The obvious drawback is that pure ice clouds may not exist in a subsaturated or supersaturated state, and no information concerning the ice crystal number concentration is available.

The new scheme now allows ice supersaturation in the 0°C to -23°C temperature range which was not possible in the previous scheme due to the diagnostic temperature dependent assumption for the liquid/ice split. Figure 2 shows a relative humidity versus temperature diagram to highlight this aspect in the previous and new versions of the scheme. Grid box mean relative humidity and temperature for cloudy points where cloud fraction is greater than 10% are plotted. The distribution of points is predominantly along the model saturation curve, which for the previous scheme follows water saturation for temperatures above freezing, mixed liquid-ice saturation between 0°C to -23°C and then ice saturation at temperatures colder than this. The occurrence of subsaturated grid box mean relative humidities highlights the ability of the model to retain cloud when the clear air humidity is below 100% due to the sub-grid heterogeneity assumption and prognostic cloud fraction variable. In addition supersaturation with respect to ice can occur in the clear air at temperatures colder than -23°C, but a discontinuity in ice supersaturation is seen at this temperature threshold (Fig. 2b). In contrast, the new scheme allows subsaturated states and ice supersaturated states in the clear air at all temperatures below 0°C with no artificial discontinuity at -23°C (Fig. 2c).

2.3.2 Ice crystal growth by deposition in mixed phase clouds

The scheme allows supercooled liquid water to exist at temperatures warmer than the homogeneous freezing threshold of -38°C. At temperatures colder than this water droplets are assumed to freeze instantaneously. When supercooled liquid and ice are coexistent, they are assumed to be well mixed and distributed uniformly through the cloud (see Rotstayn *et al.* (2000) for a discussion of alternative assumptions). The ice crystals can then grow at the expense of the water droplets through the Wegener-Bergeron-Findeisen process. If water droplets are present, the ice crystals are in an environment supersaturated with respect to ice and grow by deposition, reducing the water vapour and leading to subsaturation with respect to water. Water droplets then evaporate and the process continues with ice growth until the water droplets are completely evaporated. Thus in mixed phase clouds, the deposition process acts as a sink of cloud liquid and a source of ice cloud.

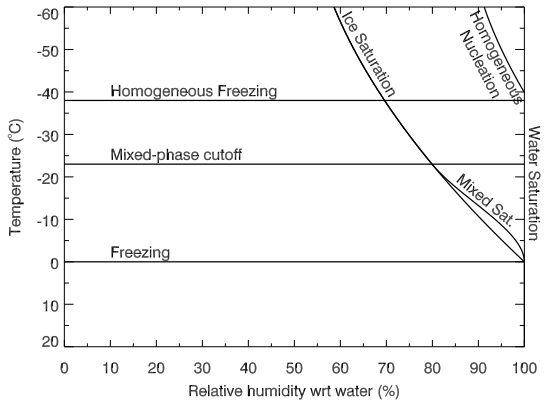

(a)

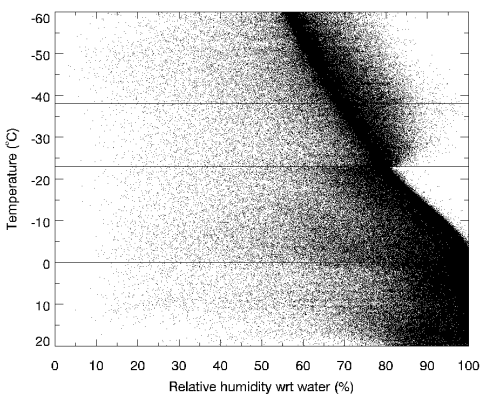

(b)

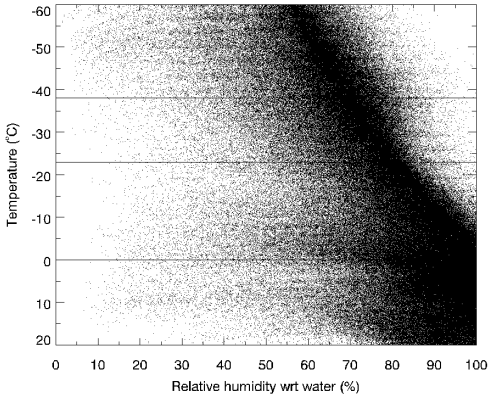

(c)

Figure 2: *Distribution of relative humidity (with respect to water) for cloudy and partially cloudy grid points as a function of temperature for a typical model forecast, (a) relevant curves for the microphysical processes in the model, (b) data from the old scheme with diagnostic mixed-phase showing the discontinuity at -23 °C, (c) data from the new scheme allowing ice supersaturation at all temperatures colder than 0 °C.*

Following Pruppacher and Klett (1997) and Rotstayn *et al.* (2000), the rate of growth of an ice crystal of mass M_i is:

$$\frac{dM_i}{dt} = \frac{4\pi C(S_i - 1)}{\alpha + \beta}, \tag{9}$$

where C is the capacitance of the particle (related to the shape) and $S_i = e/e_{si}$ is the saturation ratio with respect to ice. Terms α and β represent heat conduction and vapour diffusion respectively,

$$\alpha = \frac{L_s}{K_a T}\left(\frac{L_s}{R_v T} - 1\right) \tag{10}$$

$$\beta = \frac{R_v T}{\chi e_{si}} \tag{11}$$

where K_a is the heat conductivity of air and χ is the diffusivity of water vapour in air, which varies inversely with pressure as $\chi = 2.21/p$. If the ice crystal number concentration is N_i and the ice crystals are assumed to be monodispersed with all particles having equal diameter D_i and equal mass M_i (and therefore also equal density ρ_i), then the cloud ice specific water content $q_i = M_i N_i/\rho$. If the air is at water saturation, then $S_i = (e_{sl} - e_{si})/e_{si}$, and from (9) the rate of change of q_i is

$$\frac{dq_i}{dt} = \frac{N_i}{\rho} \frac{4\pi C}{(\alpha+\beta)} \frac{(e_{sl} - e_{si})}{e_{si}}. \tag{12}$$

The capacitance term C assumes ice crystals are spherical ($C = D_i/2$) where $D_i = (6M_i/\pi\rho_i)^{1/3}$. Elimination of C from (12) then gives

$$\frac{dq_i}{dt} = c^s_{vd} q_i^{1/3} \tag{13}$$

where

$$c^s_{vd} = \left(\frac{N_i}{\rho}\right)^{2/3} \frac{7.8}{\rho_i^{1/3}(\alpha+\beta)} \frac{(e_{sl} - e_{si})}{e_{si}}. \tag{14}$$

The analytical treatment of Rotstayn *et al.* (2000) is used, which assumes the temperature dependent quantities in (14) can be approximated as constant through the timestep. The ice condensate amount at time t can then be calculated by integrating (13) with respect to time, giving

$$q_i^t = \left(\frac{2}{3} c^s_{vd} \Delta t + (q_i^{t-1})^{2/3}\right)^{3/2} \tag{15}$$

and the deposition rate becomes, $S_{\text{dep}} = (q_i^t - q_i^{t-1})/\Delta t$.

In order to calculate the deposition rate, the ice crystal concentration is required for (14), assuming heterogeneous ice nucleation has occurred in the supersaturated air. As stated earlier, no prognostic equation for the ice crystal concentration is introduced, and thus N_i in (14) is given diagnostically, assuming the air is at water saturation, according to the Meyers *et al.* (1992) deposition-condensation-freezing nucleation parametrization:

$$N_i = 1000 exp[12.96(e_{sl} - e_{si})/e_{si} - 0.639] \tag{16}$$

The ice crystal concentration has great uncertainty but Meyers *et al.* (1992) showed (16) correlated well with continuous-flow diffusion-chamber measurements across a range of temperatures and supersaturations.

To initiate the glaciation process, at each gridbox, a minimum ice mass mixing ratio is assumed of

$$q_i^{min} = \frac{m_{i0} N_i}{\rho} \tag{17}$$

where m_{i0} is the initial mass of an ice particle and is set to 10^{-12}kg after Wilson and Ballard (1999).

Once the supercooled liquid water reservoir in the cloud is exhausted through the deposition process, there is a complication to consider. At the point the cloud becomes completely glaciated, the in-cloud vapour pressure is equal to e_{sl}. From this point the ice crystals would continue to grow by deposition of water vapour, until the in-cloud vapour pressure is reduced to the saturation value with respect to ice

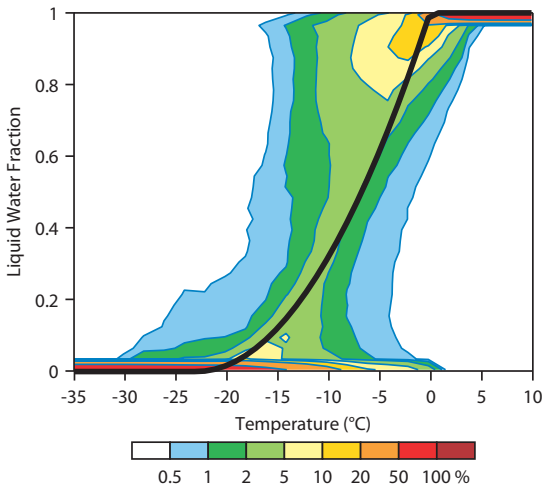

Figure 3: *Global percentage occurrence (for a given temperature) of the liquid water fraction of cloud condensate for the previous diagnostic temperature-dependent mixed-phase scheme (solid black line) and the new prognostic ice/liquid scheme (shading) for a range of temperatures (on 10 January 2011).*

(or an equilibrium value exceeding the saturation value in the presence of strong updraughts, see for example Ren and Mackenzie, 2005). However, unlike the mixed phase situation, where the "memory" for the vapour reservoir is provided by the prognostic cloud liquid water variable, there is no memory for the water vapour content in the cloudy region of the gridbox in order to model the deposition process in glaciated clouds. So, the new cloud follows the same assumption as before for pure ice cloud (see previous subsection) and the deposition of the remaining water vapour in excess of ice saturation occurs within a single timestep, bringing the cloud to exactly ice saturation.

To summarise, in mixed phase clouds with supercooled liquid water present the cloud is assumed to be exactly at saturation with respect to water (and therefore supersaturated with respect to ice), and when only ice is present, the cloud is assumed to be exactly at saturation with respect to ice. However, supersaturation is permitted in the clear sky portion of a grid cell in all cases.

It is the process of deposition that largely determines the partition between liquid and ice in mixed phase clouds in the scheme. Figure 3 shows the partition between ice and liquid cloud for an integration using the new scheme compared to the default model. It is seen that the 'S' shape is reproduced from observations (e.g. Rotstayn *et al.*, 2000). Compared to the default model which sets liquid water fraction diagnostically to zero at -23°C, there are more occurrences of liquid water at temperatures colder than this threshold. The mode of the distribution still approximately follows the temperature-dependent function, but variability is significantly increased. For example, 100% of cloud is all ice at -35°C, 100% is all liquid at +10°C, but at -10°C the cloud can vary from all ice, through varying fractions of supercooled liquid water, to all water. There is no liquid water at temperatures colder than around -38°C due to homogeneous freezing and there is more occurrence of pure ice cloud at all temperatures below 0°C. Small ice fractions (i.e. liquid water fractions just less than one) at temperatures greater than 0°C are due to the fact that ice is allowed to fall and takes a finite time to melt.

2.3.3 *Freezing and melting*

A new microphysical pathway is added to treat the melting of ice into liquid, which was not required in the previous scheme due to the diagnostic liquid/ice assumption and lack of sedimentation in the 0°C to -23°C temperature range. In addition, the process of freezing rain is included, which converts rain to snow due to the lack of a suitable, hail-like category. For the freezing of rain, the treatment is very simple, with all rain freezing in a timestep if the temperature is below 0°C, with a check to ensure that the temperature does not increase above this threshold due to the latent heating of the process. The melting of ice and snow are treated in a similar way to the diagnostic snow variable in the previous scheme, allowing the melting to cool the gridbox to 0°C over a specified timescale. These processes are currently treated explicitly.

2.3.4 *Sedimentation*

The numerical formulation of the sedimentation process (falling hydrometeors due to gravity) follows the forward-in-time upstream approach as in the previous version. The rain, snow and ice hydrometeor categories are allowed to sediment.

With the potential for hydrometeors to settle through many model layers in a single timestep, using a mass related fall speed formulation ($V_x = F(q_x)$) can lead to numerical 'shocks' when long timesteps are necessary (e.g. Wacker and Seifert, 2001). Thus the fallspeeds are set to a constant ($V_{i0} = 0.15$ m s^{-1}, $V_{s0} = 1$ m s^{-1}, $V_{r0} = 4$ m s^{-1}) to avoid this. However, the fallspeed for ice and snow are adjusted to account for variations in temperature and pressure as derived by Heymsfield and Iaquinta (2000),

$$V_x = V_{x0}\left(\frac{p}{p_{\text{fall}}}\right)^{-0.178}\left(\frac{T}{T_{\text{fall}}}\right)^{-0.394} \tag{18}$$

where $p_{\text{fall}} = 30000$ Pa and $T_{\text{fall}} = 233$ K.

Sedimentation of ice in the previous scheme was not active in the 0°C to -23°C temperature range and was gradually increased to 0.15 m s^{-1} at temperatures colder than -23°C. Therefore the new scheme has an additional sink of ice due to sedimentation in this temperature range that was not present before. This reduces the ice water content compared to the previous scheme (as shown in Section 3.2).

2.3.5 *Autoconversion*

There are two changes to the autoconversion treatment. Previously, the autoconversion of ice to snow only operated in the pure ice phase (T<-23°C) with all cloud condensate treated by the rain autoconversion process for temperatures warmer than this threshold. This temperature threshold approach was used to minimize impact on the cloud scheme when the snow autoconversion was introduced along with the implicit numerical approach in Cycle 31r1. The surface precipitation and model hydrological cycle is very sensitive to the treatment of the autoconversion in the mixed phase, since the collection-term (rain and snow collecting cloud droplets) make the scheme highly nonlinear.

With separate cloud liquid and ice variables, there is no need to retain this artificial temperature threshold in the new scheme, and now the snow autoconversion works to convert ice to precipitating snow, irrespective of temperature, and the warm-phase autoconversion only takes liquid cloud into account. The adjustment factor (Sundqvist, 1978) that accounts for the Bergeron-Findeisen process is also removed as this process is now represented explictly by the deposition term described above.

The rate of generation of precipitation is written as

$$S_{\text{auto}}^{\text{rain}} = ac_0 q_{\text{l}}^{\text{cld}} \left[1 - \exp\left\{ -\left(\frac{q_{\text{l}}^{\text{cld}}}{q_{\text{l}}^{\text{crit}}} \right)^2 \right\} \right] \tag{19}$$

where $q_{\text{l}}^{\text{cld}}$ is the in-cloud value of cloud water content (q_{l}/a), a is the cloud fraction, c_0^{-1} represents a characteristic time scale for conversion of cloud liquid droplets into rain drops and $q_{\text{l}}^{\text{crit}}$ is a typical cloud water content at which the generation of precipitation begins to be efficient. The critical liquid water content is different over ocean and land to take account of the differences in cloud condensation nuclei (CCN) in clean and polluted air. Cleaner air over the ocean has fewer CCN, hence larger drops and an onset of precipitation at lower cloud liquid water contents than in the more polluted air over land. These two disposable parameters are defined as

$$c_0 = c_0^* F_1 \tag{20}$$

and

$$q_{\text{l}}^{\text{crit}} = \frac{q_{\text{l}}^{\text{crit}*}}{F_1} \tag{21}$$

to take into account the effect of collection (accretion) of cloud droplets by raindrops falling through the cloud (F_1). Here F_1 is defined as

$$F_1 = 1 + b_1 \sqrt{P_{\text{loc}}} \tag{22}$$

where P_{loc} is the local cloudy precipitation rate ($P_{\text{loc}} = P^{\text{cld}}/a_P^{\text{cld}}$) and a_P^{cld} is the precipitation fraction overlapping with cloud (see section on precipitation below). For warm-phase autoconversion, the rate coefficient is $c_0^* = 1.67 \times 10^{-4}$ s^{-1} and the critical water content $q_{\text{l}}^{\text{crit}*}$ is set to 3×10^{-4} kg kg^{-1} over ocean and 5×10^{-4} kg kg^{-1} over land. For cold-phase (ice to snow) autoconversion, the rate coefficient (c_0) is based on Lin *et al.* (1983), $c_0 = 10^{-3} e^{0.025(T-273.15)}$ and the critical ice water content $q_{\text{i}}^{\text{crit}}$ is set to 4×10^{-5}kg kg^{-1}.

The critical threshold is a factor of ten smaller for the cold-phase autoconversion and the autoconversion rate is a factor of 5 higher, so this change results in a much more efficient sink of ice cloud and therefore a significant decrease in the cloud ice contents is expected in the 0 to -23°C temperature range (as shown in Section 3.2).

2.3.6 Precipitation evaporation/sublimation

Precipitation processes are treated separately in clear and cloudy skies. The microphysical processes in these two regions are very distinct from each other, with conversion, collection and accretion processes being relevant in clouds whereas evaporation of precipitation is the relevant process outside clouds.

Whereas cloud fraction (for cloud liquid and cloud ice) is a prognostic variable, precipitation fraction (for rain and snow) is still treated diagnostically. The treatment of precipitation fraction in the previous cloud scheme (Jakob and Klein, 2000) in IFS cycles prior to 36r4 needed to be updated for the new prognostic microphysical treatment, since snow and rain water content are now prognostic variables and can survive from one timestep to the next. So the previous complex two-stream treatment is replaced by a simpler treatment where the total precipitation fraction a_P (the sum of the in-cloud precipitation fraction a_P^{cld} and the clear sky precipitation fraction a_P^{clr}) is calculated using a maximum-random overlap treatment of the cloud fraction, so that at level k:

$$a_{P,k} = 1 - \left(\frac{(1 - a_{P,k})(1 - MAX[a_k, a_{k-1}])}{1 - MIN[a_{k-1}, 1 - \varepsilon]} \right), \tag{23}$$

where ε is equal to a small number (10^{-6}) and a_k is the cloud cover at level k. The clear sky precipitation fraction is then given by

$$a_P^{clr} = a_P - a. \tag{24}$$

The precipitation flux is proportionally divided between the clear-sky and the in-cloud component, implying a greater artificial subgrid horizontal flux than in the previous diagnostic scheme. However, this is unavoidable without additional prognostic variables to represent the clear-sky and in-cloud precipitation coverages.

For the evaporation process, the previous scheme assumed horizontal homogeneity of the precipitation. Thus in a sub-cloud layer the clear sky precipitation fraction ($a_P^{\rm clr}$) remained constant while the flux reduced due to evaporation. Only if the precipitation reached zero did the clear sky fraction also reset to zero. This treatment resulted in very discrete behaviour of the vertical profile of $a_P^{\rm clr}$. The new scheme does assume sub-grid heterogeneity in the clear sky precipitation flux, which corresponds to a reduction in the total precipitation fraction proportionally to the reduction in precipitation flux by the evaporation process. This leads to much smoother vertical profiles of precipitation coverage. Note that the ad-hoc threshold to inhibit evaporation in moist atmospheres is retained in the revised scheme.

Rain and snow are prognostic variables and can be advected by the wind out of the column that they were produced, but precipitation fraction is still a diagnostic. Therefore a precipitation fraction needs to be specified when there is no cloud fraction in the column above. At present, this is set as a minimum precipitation coverage of 30%.

2.4 Impacts on other parametrization schemes

2.4.1 Radiation scheme

In the previous versions of the IFS (pre-36r4), the radiation scheme only took account of the liquid and ice cloud water contents and cloud fraction in the radiative calculations; the impacts of precipitation were neglected. This is a reasonable assumption as cloud particles dominate radiative absorption, scattering and emission, and cloud is already present in the grid column when precipitation is generated. However, precipitation may have a non-negligible impact on the radiation. This particularly applies to the *snow* hydrometeor category. In the model the *ice* and *snow* categories represent the small and large particles respectively, as an approximation to the continuous frozen particle size spectrum. The split between ice and snow in the model is rather arbitrary in terms of the impact on radiation and it is therefore not unreasonable to include the combined effect of ice and snow. So the new scheme includes the snow prognostic variable as well as cloud ice and cloud liquid water (rain is still neglected for now). The diagnostic precipitation fraction is not yet utilised so the snow is added to the ice cloud wherever there is ice cloud present, to form a total ice water content as input to the scheme. The radiative calculations are then performed on this total ice water content rather than the ice cloud alone.

In the IFS model the ice particle effective radius is a function of temperature and ice water content, based on analysis of observational aircraft data from Sun and Rikus (1999) (revised by Sun, 2001), which covers a range of particle sizes. The effective radius is currently limited between a minimum of 20+40cos($latitude$) μm and a maximum of 155μm. A factor of 0.64952 is used to convert from effective radius to particle diameter. At present, the same optical properties are used for the ice and snow particles; Fu (1996) for the shortwave optical properties and Fu *et al.* (1998) for the longwave spectral emissivity.

Combining the ice and snow water contents and using the existing parametrization of frozen particle

properties is a first implementation with potential for further development in the future. There are clearly a number of assumptions that could be improved regarding the radiative impacts of cloud and precipitation, including separate assumptions for the ice (assuming pristine crystals) and snow (assuming aggregates) but there are also many uncertainties in particle sizes, shapes and optical properties to deal with. In addition the impact on radiation from stratiform rain, and cloud and precipitation from the convective parametrization (representing convective cores) could be investigated.

2.4.2 Convection scheme

For the moment, the input to the cloud scheme from the convection parametrization remains unchanged. The detrained cloud water is divided into liquid or ice according to the previous diagnostic temperature dependent mixed phase assumption and the treatment of the subsidence term still uses the mixed definition of saturated specific humidity.

2.4.3 Vertical diffusion

The vertical diffusion scheme combines vapour, liquid and ice into a total water quantity, which undergoes mixing, and is then divided according to the mixed liquid/ice definition of saturated specific humidity into vapour and cloud mass. In the previous scheme the cloud mass was separated diagnostically into liquid and ice according to temperature and tendencies calculated appropriately. In the new scheme, different options for the proportion of liquid and ice created or evaporated by the mixing could be chosen, but initially the simplest approach was implemented; dividing the tendency of total water into liquid and ice in the same proportions as the input cloud liquid and ice before mixing takes place. For the case where there is initially no cloud in the grid box and the diffusion scheme creates cloud, the cloud tendency is all in the liquid phase.

2.4.4 Semi-Lagrangian advection

In the standard operational model, the liquid and ice cloud condensate variables are treated differently to the other variables in the advection scheme, since gradients can be large and the scheme uses a linear interpolation to avoid generation of negative values in regions of strong gradient. For consistency this interpolation method is retained for the liquid, ice, rain and snow prognostic variables in the new scheme.

3 Results

The new scheme in IFS Cycle 36r4 has a number of impacts on the IFS model forecasts of cloud and precipitation, some of which are described in more detail here and others, including the validation of supercooled liquid water, the radiative impact of snow, and precipitation over orography, are left to more in depth studies in follow-on reports. First, an overview of the changes to the “climate” of the model cloud, precipitation and radiation fields are described, followed by a discussion of the improved global distribution of ice and snow, and the improved skill of precipitation forecasts.

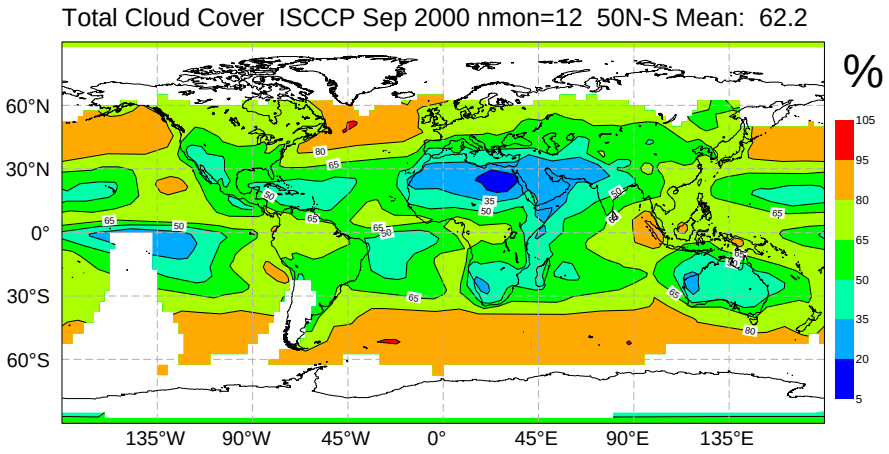

(a)

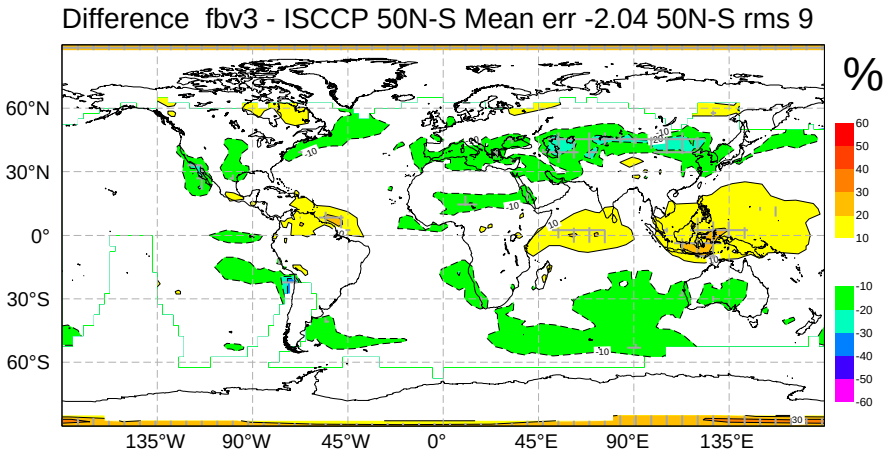

(b)

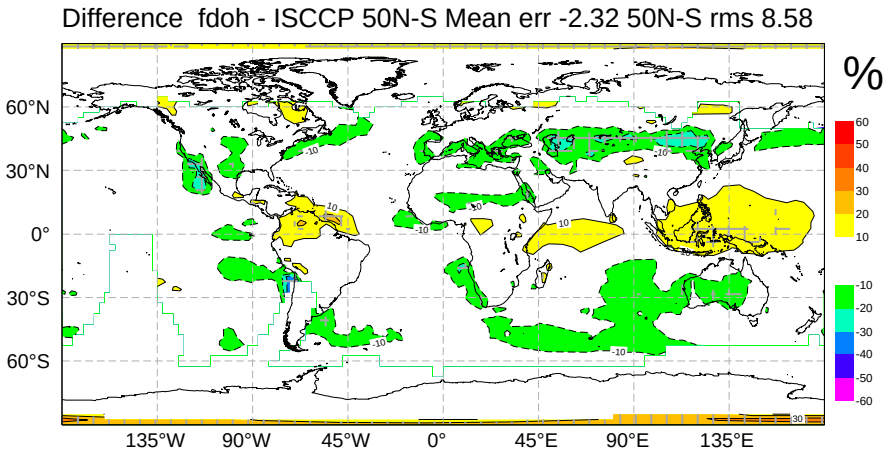

(c)

Figure 4: *Annual mean total cloud cover (September 2000 to August 2001) for (a) ISCCP observational dataset, (b) IFS Cycle 36r3 with previous cloud scheme and (c) with the new cloud scheme. The mean error and root mean square error (model - observations) are in the title line for the two model versions. Hatched areas indicate regions of higher statistical significance.*

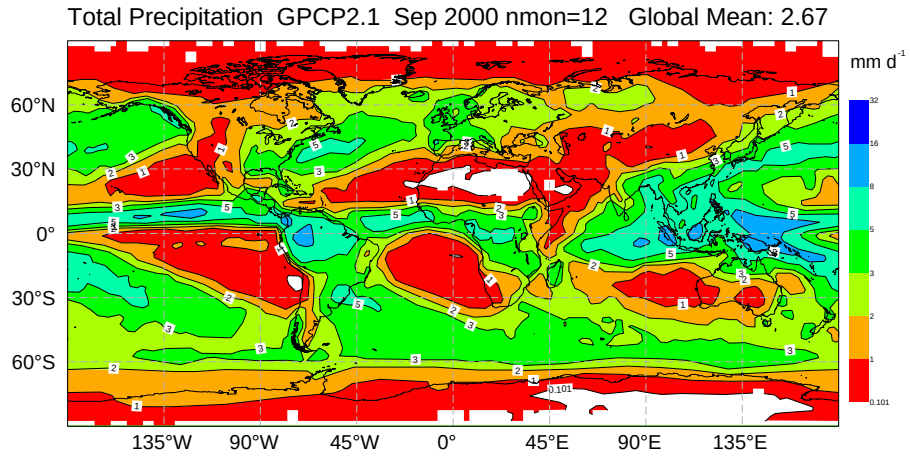

(a)

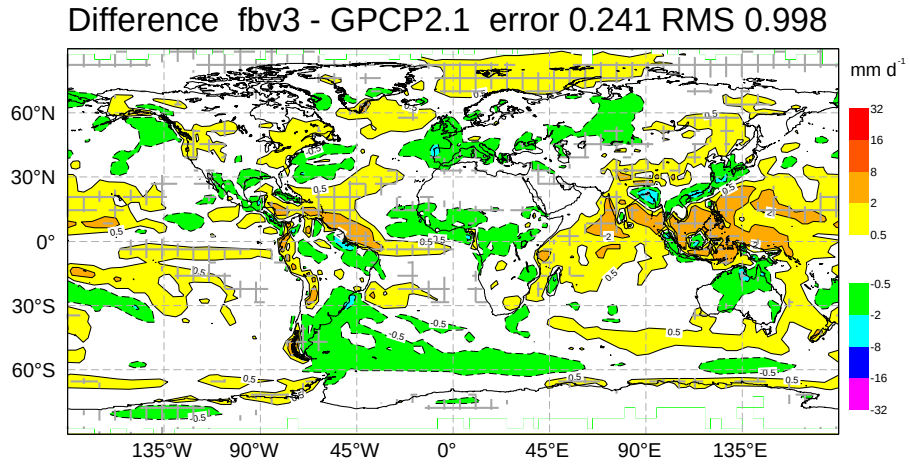

(b)

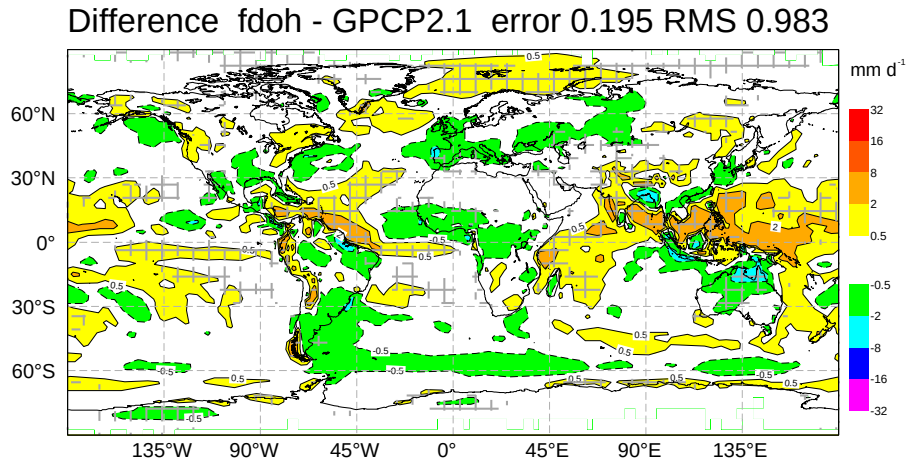

(c)

Figure 5: *As Figure 4 but for annual mean precipitation (September 2000 to August 2001) for (a) GPCP2.1 observational dataset, (b) IFS Cycle 36r3 with previous cloud scheme and (c) with the new cloud scheme.*

3.1 Impact on model climate

Figures 4 to 7 show global comparisons of IFS Cycle 36r3, with the previous cloud scheme and with the new cloud scheme, against observation-based datasets for total cloud cover, precipitation and top-of-atmosphere net shortwave and net longwave radiation. The model forecasts are 13 month integrations starting in August 2000, with the first month discarded to create 12 month annual means. Four integrations with different start dates are averaged together to increase statistical significance. The resolution of the model has a T159 spectral truncation equivalent to a grid-spacing of about 125 km; a resolution used for the seasonal forecasting system (System 3) at ECMWF. All observational datasets are averaged over the same time period. Although limited to one year, these simulations do provide useful information on the systematic errors of the model "climate".

Generally, the spatial patterns of the systematic errors are very similar in both versions of the cloud scheme, but the root mean square errors are reduced for all fields with the new scheme. The total cloud cover is reduced in the tropics, and slightly increased in the extra-tropics, both reducing the differences with the ISCCP dataset (International Satellite Cloud Climatology Project (D2), Rossow and Schiffer, 1991; Rossow *et al.*, 1996). This results in a slight increase in the mean error, but an overall reduction in the r.m.s. from 9% to 8.6% cloud cover (Fig. 4). The total precipitation difference against the Global Precipitation Climatology Project (GPCP2.1) dataset (Adler *et al.*, 2003) has a complex spatial structure relating to different meteorological regimes (Fig. 5). However, both the mean error and r.m.s. are reduced slightly with the new scheme, the latter from approximately 1.0 to 0.98 mm day^{-1}.

Both the mean error and r.m.s. of the top-of-atmosphere net shortwave and longwave radiation versus the CERES observations (Clouds and the Earth's Radiant Energy System, Wielicki *et al.*, 1996, 2006) show reductions with the new scheme. The negative shortwave bias in the Tropics (Fig. 6) indicates too much reflection and this is reduced with lower liquid water paths in the new scheme. However, the positive shortwave bias in the Southern Hemisphere (SH) is slightly worse, indicating the new scheme may have reduced the supercooled liquid water too much in the cold cloud south of 50°S (Note this has been addressed in later model cycles and will be reported on separately). Despite the higher bias in the SH, the overall r.m.s. is reduced from 16.5 to 15.7 Wm^{-2}. The longwave radiation has similar patterns in both simulations with a reduction in r.m.s from approximately 7.2 to 7.0 Wm^{-2} (Fig. 7).

3.2 Impact on global distribution of cloud ice and snow

Modifications to the representation of ice and snow in the new scheme result in significant changes to the three-dimensional distribution of frozen particles in the model. As mentioned earlier, the two-category approach is a way of representing small and large particles in the scheme. Smaller ice particles with low fall velocities associated with cloud that grows primarily by deposition are represented by the 'ice' category and 'snow' represents larger ice particles with higher fall velocities that grow through collection (aggregation). The process of 'autoconversion' is used to represent the onset of broadening of the particle size distribution through aggregation, leading to conversion of mass from the 'ice category' to the 'snow category'. The latter, representing larger particles, then precipitates at a faster rate.

Previously, the autoconversion of ice to snow only operated in the pure ice-phase temperature zone (colder than -23°C) with all cloud condensate treated by the less efficient rain autoconversion process at temperatures warmer than this threshold. Another necessary condition of the diagnostic approach to the mixed phase in the previous scheme was an assumption of zero fall velocity for ice cloud between 0°C and -23°C which then gradually increased in the pure-ice phase at colder temperatures above. These two restrictions meant the only sink of ice in the mixed-phase zone was the repartitioning into liquid and ice

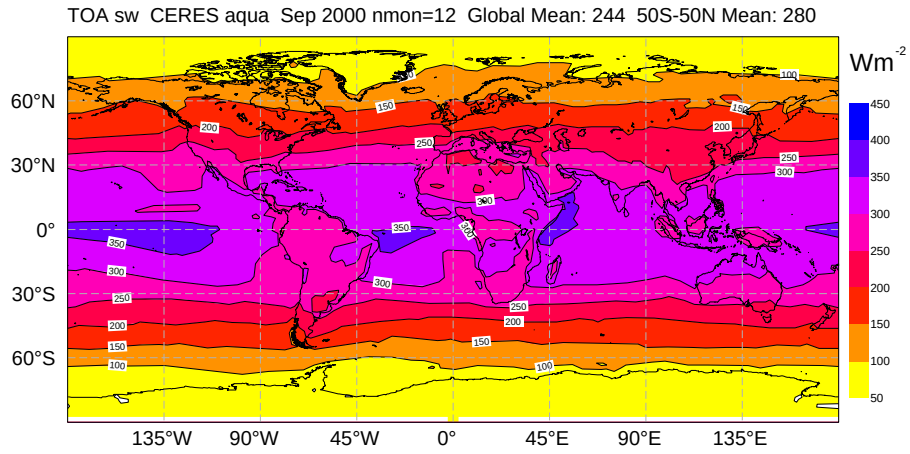

(a)

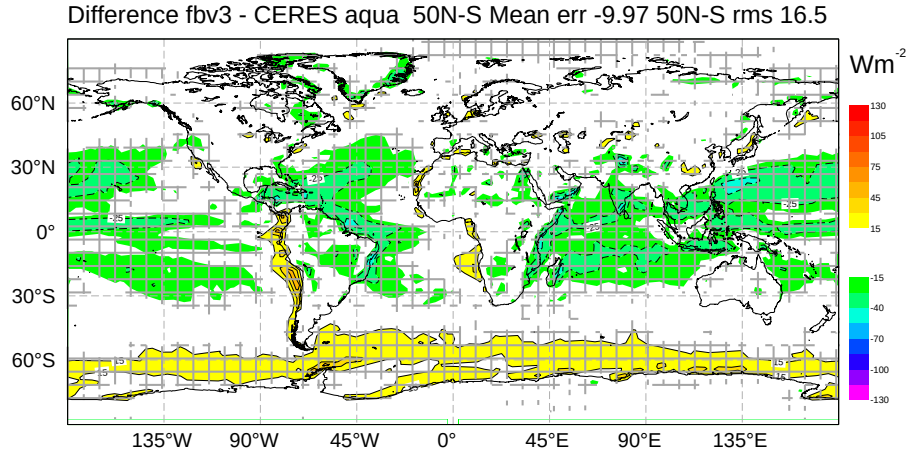

(b)

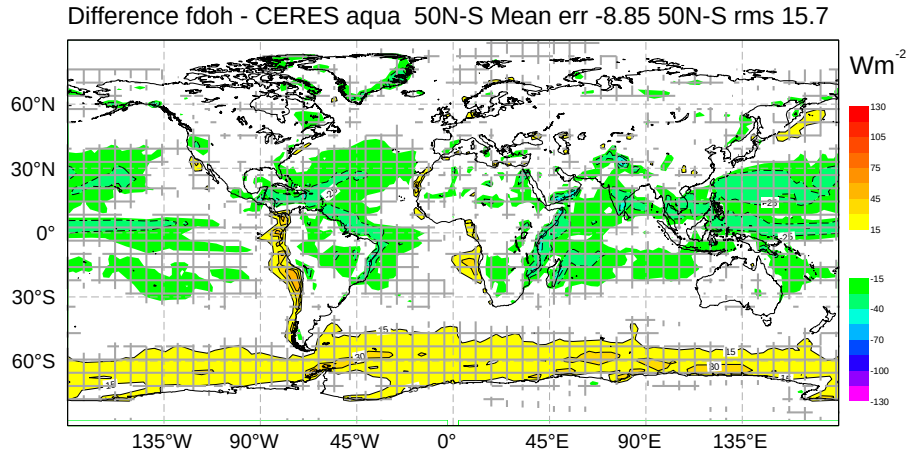

(c)

Figure 6: *As Figure 4 but for annual mean top-of-atmosphere net short-wave radiation (September 2000 to August 2001) for (a) CERES observational dataset, (b) IFS Cycle 36r3 with previous cloud scheme and (c) with the new cloud scheme.*

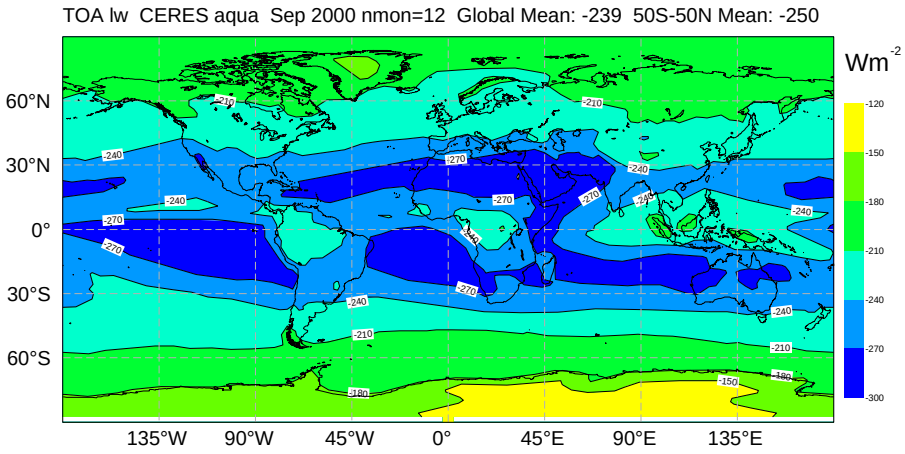

(a)

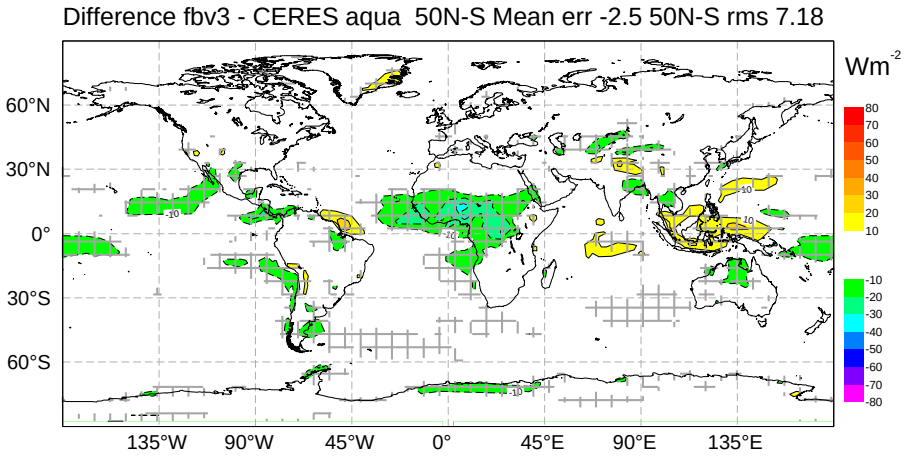

(b)

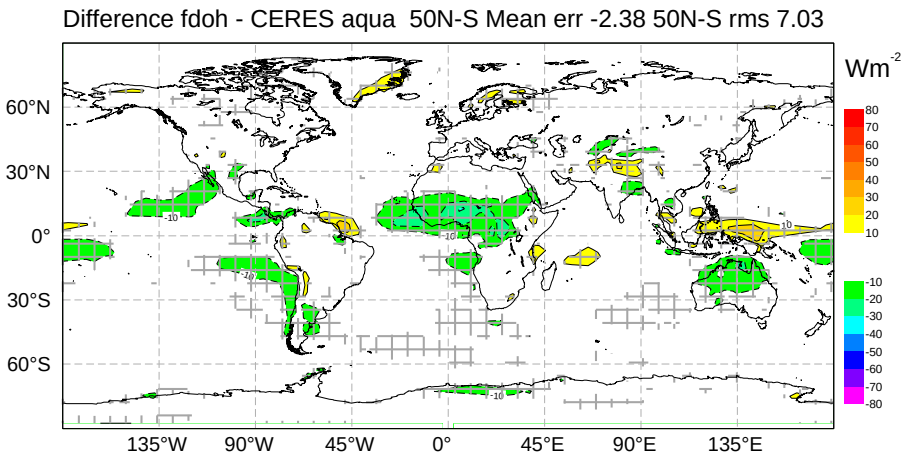

(c)

Figure 7: *As Figure 4 but for annual mean top-of-atmosphere net long-wave radiation (September 2000 to August 2001) for (a) CERES observational dataset, (b) IFS Cycle 36r3 with previous cloud scheme and (c) with the new cloud scheme.*

at every timestep and this led to artificially high ice cloud mass in the mixed-phase zone.

As discussed in Section 2, the new scheme now has a consistent treatment of autoconversion and sedimentation for the new prognostic ice variable throughout the temperature range and therefore avoids any discontinuities at $-23°$C and significantly reduces the amount of ice at temperatures warmer than $-23°$C. Figure 8 shows the zonal cross section of the annual mean cloud ice content for the previous cloud scheme, the new scheme and an estimate derived from the CloudSat radar (Austin (2007), 2B-CWC-RO Version 4 ice water content product). All 1.7 km CloudSat footprint profiles that are estimated to be either precipitating or convective in the observation data have been removed in order to capture the 'ice cloud' part of the total cloud mass (Ma *et al.*, 2012, Li *pers. comm.*). An alternative method of partitioning the total CloudSat derived ice mass into small ($< 100\mu$m) and large particles ($> 100\mu$m) gives a similar result (Waliser *et al.*, 2011).

At mid- and high latitudes the ice water content in the previous cloud scheme (Fig. 8a) is significantly higher relative to the CloudSat estimate (Fig. 8c), but this is improved in the revised scheme (Fig. 8b). Both model versions produce ice cloud down to the surface, which is lacking in the CloudSat observations due to signal attenuation, removal of signals contaminated with surface backscatter, and the mixed-phase partitioning assumption in the CloudSat data processing which assumes all ice at -20°C linearly decreasing to all liquid at 0°C. The latter assumption also means that the ice water content is uncertain in the CloudSat cross section (Fig. 8c) in the 0°C to -20°C temperature range. However the lower maximum peak at about 500hPa in the tropics in the previous cloud scheme (Fig. 8a) is not present in the CloudSat data and is highly likely to be an artificial characteristic of the diagnostic mixed-phase assumptions as discussed above. The new scheme (in IFS Cy36r4) underestimates the ice water content compared to CloudSat above 700hPa, but this is likely to be improved in the future with modifications to the ice fall velocity.

Figure 9 shows the geographical distribution of the annual mean vertically integrated cloud ice water path from the previous cloud scheme and the combined prognostic ice and snow water path from the new scheme, as well as the estimated *total* ice water path derived from CloudSat. In the extra-tropics there is good agreement between the spatial distribution and magnitude of the total stratiform ice and snow water path from the new scheme and the observed estimate. The differences in the tropics over Africa, South America and the Inter-Tropical Convergence Zone (ITCZ) are where precipitation from deep convection dominates in the observations. Ice and snow in convective cores are currently not included in the model output for deriving ice water path, and this, along with the interaction of convective cores with the radiation, are potential areas for future research.

The change in the distribution and amount of ice cloud and inclusion of radiatively active snow has important radiative impacts. Consequently, as seen in the previous section, the root mean square error of both net shortwave and longwave annual mean radiative fluxes at the top of the atmosphere are reduced in the new scheme compared to observations from the CERES satellite instruments. Further analysis of the impacts of cloud ice and snow on the radiative heating of the troposphere is beyond the scope of this report and will be reported in the future.

3.3 Impact on forecast precipitation

Both rain and snow precipitation are now prognostic variables, which are stored from timestep to timestep, precipitate with a terminal fall velocity and are advected by the wind. As before, the precipitation processes of generation through autoconversion from cloud, collection of cloud particles (accretion, aggregation), melting (from snow to rain) and evaporation are all included. However, there is no longer

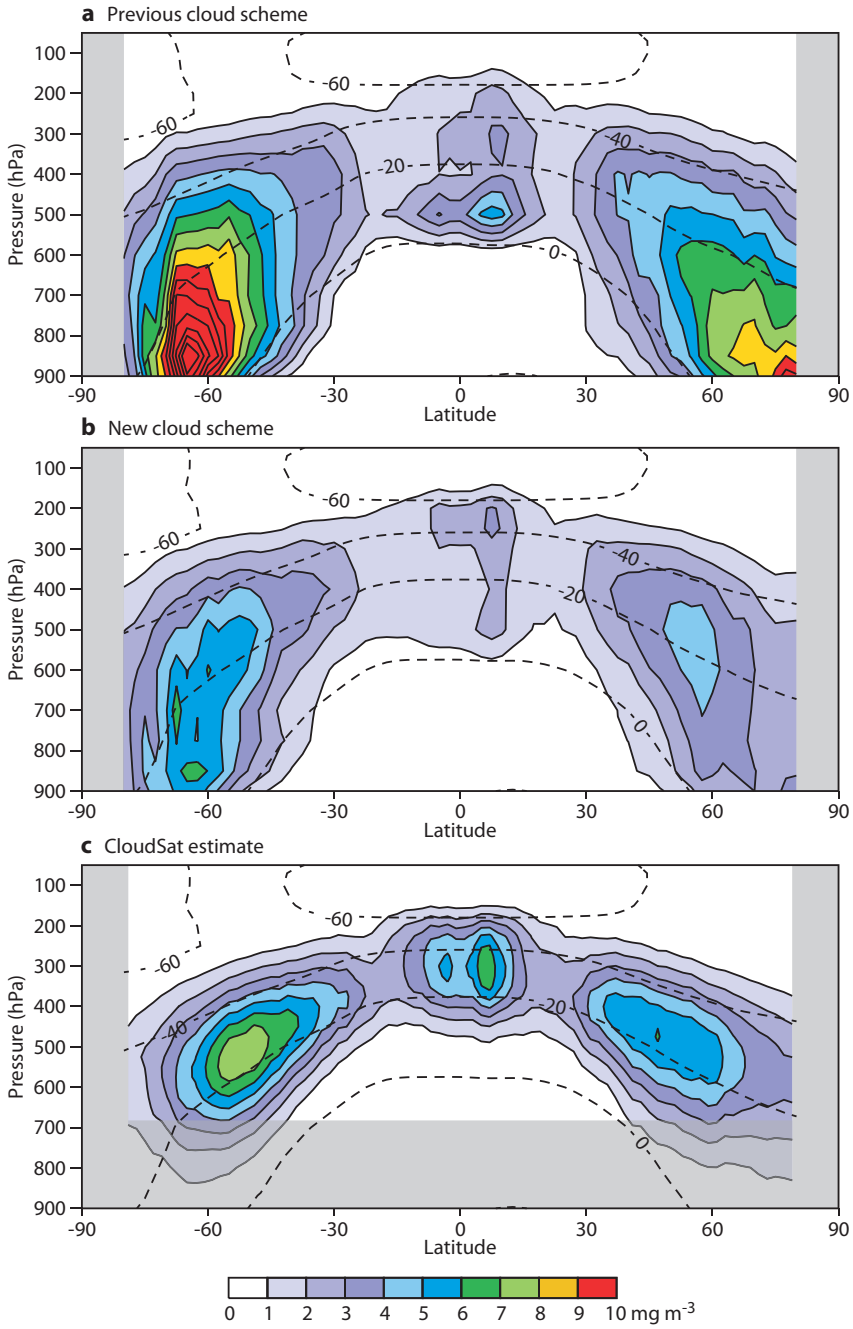

Figure 8: *Zonal cross-section of annual mean cloud ice (mg m-3) for (a) the previous IFS cloud scheme with a diagnostic mixed phase, (b) the new IFS cloud scheme with a consistent treatment of cloud ice at all temperatures and (c) the estimate derived from CloudSat (82°S to 82°N) filtering out all observed precipitating and convective profiles to obtain a closer equivalent to the model cloud ice field (Li, pers. comm.). Annual mean temperature is shown as dashed contours (°C). The shading indicates areas where data is absent or particularly uncertain.*

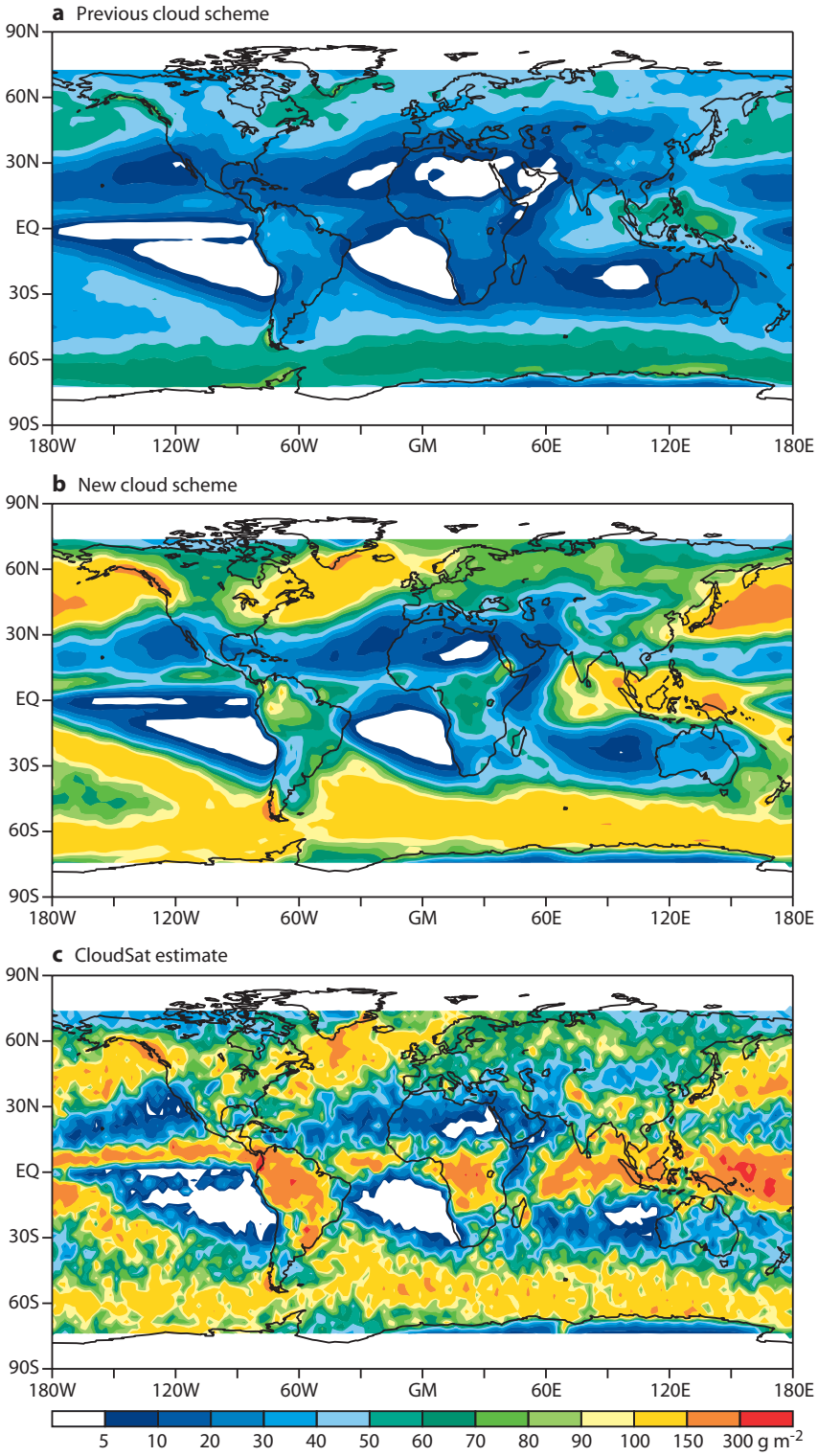

Figure 9: *Annual mean vertically integrated ice water path (g m-2) for (a) radiatively active cloud ice from the previous cloud scheme, (b) radiatively active total cloud ice and snow from the new cloud scheme, and (c) estimate derived from CloudSat (August 2006 to July 2007), (Waliser et al., 2009).*

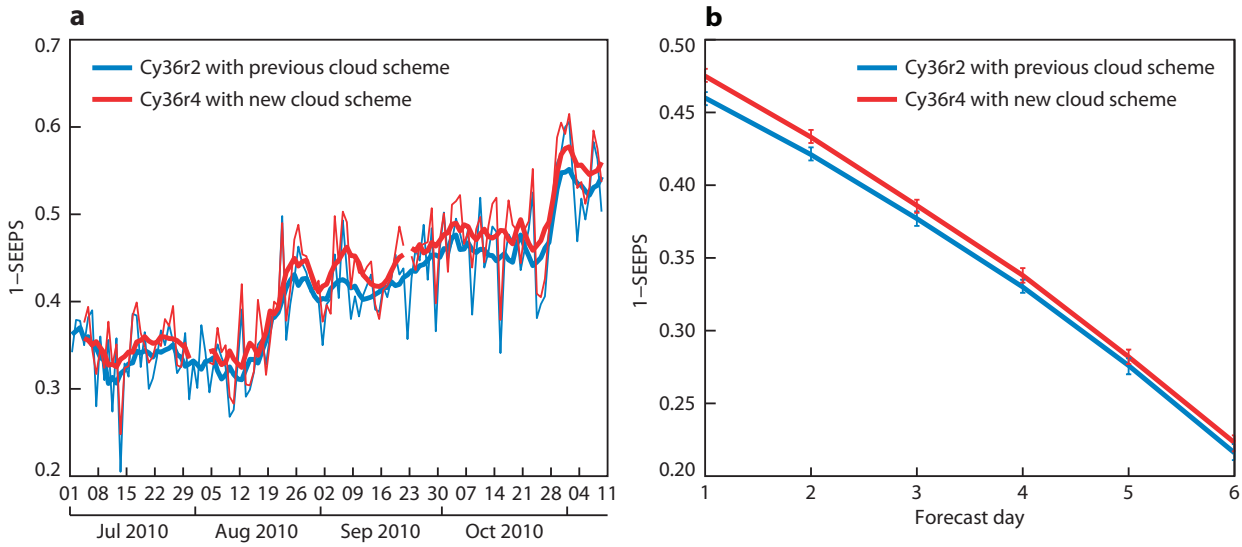

Figure 10: *(a) Global precipitation skill score (1-SEEPS) for Cy36r4 with the new cloud scheme and the previous operational Cycle Cy36r2 for the period 1 July to 9 November 2010 (24- to 48-hour forecast accumulations from 00 UTC forecasts). Thin lines: daily values, bold lines: running weekly average. (b) Global 1-SEEPS score averaged over the same period as a function of lead time (24-hour accumulations from 12 UTC forecasts). Higher values represent higher skill. Error bars show 95% confidence intervals.*

an instantaneous response of surface precipitation to the microphysical processes in the local atmospheric grid column above. With the prognostic representation, precipitation can be blown by the wind as it falls over multiple timesteps, which results in a spatially and temporally smoother precipitation field.

The advection of snow by the wind can be particularly significant in regions of orographic forcing producing persistent geographically locked precipitation. With a diagnostic precipitation scheme, precipitation often falls on the upslope and peaks of the orography as an instantaneous response in the vertical to the local forcing, whereas the effect of horizontal advection by the atmospheric winds results in a downstream shift of the precipitation towards the lee of the orography and a different hydrological catchment. This effect is more significant for snow than for rain, due to the slower fall speed of snow particles and potentially longer residence time in the atmosphere. This orographic effect can be seen in the model, for example over the Alps, but the precipitation changes over orography require a detailed evaluation and are left to a follow-on study.

The changes in the new scheme contribute to a significant improvement in regional and global precipitation skill, shown for example by the 1-SEEPS score in Figure 10. SEEPS (Stable Equitable Error in Probability Space) is a new supplementary headline score at ECMWF used for verification of deterministic precipitation forecasts against SYNOP observations (Rodwell *et al.*, 2010, 2011). It is an equitable score using three categories; 'dry', 'light precipitation' and 'heavy precipitation', defined by the local climatology (30 year climatology of SYNOP station observations). The SEEPS score varies between 0 and 1, and the value of 1-SEEPS is often used so that higher values correspond to higher skill. The actual value of a perfect forecast of the 1-SEEPS score is 1, and the expected value of a random or climatological forecast is 0. In practice, the representativity error of the grid-box area versus point location of the SYNOP observations is estimated to be about 0.2, so a value of 0.8 for the 1-SEEPS score would be the maximum achievable at the current operational resolution. Figure 10 shows a consistent improvement of Cycle 36r4 with the new cloud scheme from day to day (Fig. 10a) and with forecast lead time (Fig. 10b).

4 Concluding Summary

The upgrade to the representation of cloud and precipitation in the IFS has significantly modified the cloud parametrization in terms of the number of prognostic variables, formulation of mixed-phase and precipitation processes and cloud scheme numerics. The number of prognostic variables has increased from two (cloud fraction, cloud condensate) to five (cloud fraction, cloud liquid water, cloud ice, rain and snow). Liquid and ice cloud condensates are now determined by explicit microphysical processes rather than by a fixed function of temperature, resulting in wider variability of supercooled liquid water occurrence. The representations of ice and ice supersaturation in the mixed phase temperature range (0°C to -23°C) are improved and snow is now radiatively active. Rain and snow can be advected by the wind and precipitation skill is improved.

Overall, this has been a major change to the representation of moist physics and a significant milestone towards a more physically based cloud and precipitation parametrization scheme in the IFS model. The parametrization framework is now more appropriate for a wider range of model resolutions and is closer to the typical single-moment schemes used in higher-resolution limited-area NWP and cloud resolving models (CRMs).

There are many opportunities for further development of the scheme and the focus will shift towards improving the formulation of cloud and precipitation microphysical processes to provide a stronger physical basis, improved internal consistency and a more direct link to observable parameters such as particle size distributions and particle characteristics. Ongoing evaluation against a wide range of ground based and satellite observations is a further vital activity for continued parametrization development in the IFS and improved forecasts of cloud and precipitation in NWP.

Acknowledgements

The authors would like to thank Anton Beljaars, Jean-Jacques Morcrette and colleagues at ECMWF for many informative discussions, Frank Li and Duane Waliser (JPL) for the processed CloudSat data, Thomas Haiden for the precipitation skill score comparison and Rob Hine for help with the figures. We acknowledge the NASA CloudSat project for providing the original data from CloudSat and the ISCCP project, GPCP project and CERES mission for the observational datasets.

Appendices: Technical notes

A1 Initialising the new rain/snow fields

There is a new logical INIRAINSNOW that needs to be set in the configuration file config.h in section ”inidata” at IFS Cycle 36r4 onwards which determines whether the model will initialise the new prognostic rain and snow fields from input fields if available, or otherwise initialise to zero.

INIRAINSNOW=false

if there is no existing rain and snow data for initialisation, in which case the prognostic rain and snow fields will be initialised to zero.

INIRAINSNOW=true

if the rain and snow fields are to be initialised from archived MARS data. The logical is set by prepIFS, defaulting to false if starting from initial fields from model cycles pre-36r4, but defaults to true if starting from initial fields from model cycles 36r4 onwards. It takes about 6 hours for the model to spin-up the snow and rain fields when initialised to zero at the beginning of a forecast run (Figure 11 shows an example).

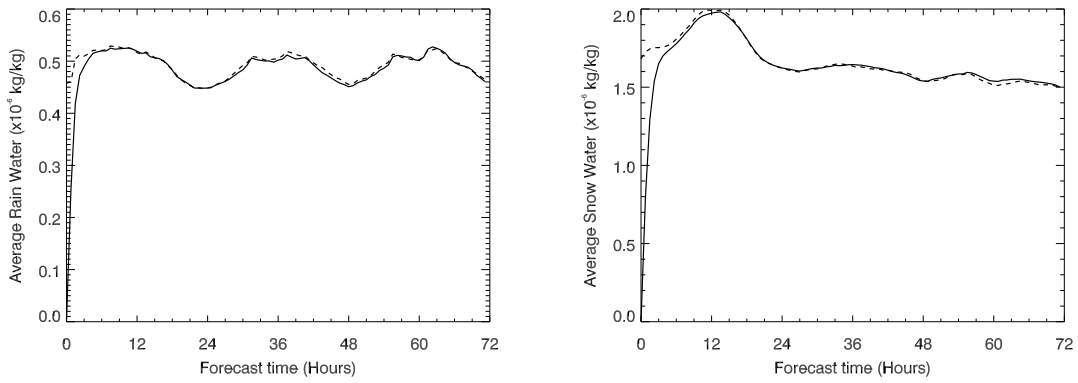

(a) (b)

Figure 11: *Evolution of the global average (a) rain and (b) snow prognostic fields for an example T255L91 forecast run (72 hours) when initialised to zero (solid line) compared to initialisation with rain/snow fields from the previous forecast during an analysis cycle (dashed line). The spin-up period is about 6 hours.*

A2 Cloud and precipitation diagnostics

The Grib codes for the ice and liquid water prognostic variables remain unchanged. The new rain and snow prognostic variables are available on model levels and have new allocated Grib codes in Grib Table 128. There are also two new single level diagnostics available for the vertically integrated rain and snow water contents (TCRW, TCSW) in Grib Table 228. A list of many of the cloud and precipitation related diagnostics is included below.

3D fields (Grib Table 128 unless specified):

Grib code	Short name	Description	Units
248	CC	Cloud fraction	(0-1)
246	CLWC	Cloud liquid specific water content	(kg kg^{-1})
247	CIWC	Cloud ice specific water content	(kg kg^{-1})
75	CRWC	Precipitation rain specific water content	(kg kg^{-1})
76	CSWC	Precipitation snow specific water content	(kg kg^{-1})
130	T	Temperature	(K)
133	Q	Specific humidity	(kg kg^{-1})
157	RH	Relative humidity (only available on pressure levels)	(%)

2D fields (Grib Table 128 unless specified):

Grib code	Short name	Description	Units
164	TCC	Total cloud cover	(0-1)
186	LCC	Low cloud cover	(0-1)
187	MCC	Mid-level cloud cover	(0-1)
188	HCC	High cloud cover	(0-1)
78	TCLW	Total column liquid water	(kg m^{-2})
79	TCIW	Total column ice water	(kg m^{-2})
228089	TCRW	Total column rain water	(kg m^{-2})
228090	TCSW	Total column snow water	(kg m^{-2})
142	LSP	Accumulated large-scale (stratiform) precipitation (rain+snow)	(m)
144	SF	Accumulated snowfall (stratiform + convective)	(m)
50	LSPF	Accumulated precipitation fraction	

References

Adler, R. F., Susskind, J., Huffman, G., Bolvin, D., Nelkin, E., Chang, A., Ferraro, R., Gruber, A., Xie, P.-P., Janowiak, J., Rudolf, B., Schneider, U., Curtis, S. and Arkin, P. (2003). The version-2 Global Precipitation Climatology Project (GPCP) monthly precipitation analysis (1979-present.). *J. Hydrometeorol.*, **4**, 1147–1167.

Austin, R. T. (2007). Level 2B radar-only cloud water content (2B-CWC-RO) process description document. *Cloudsat Projects Report*, p. 24.

Bouniol, D., Protat, A., Delanoė, J., Pelon, J., Piriou, J. M., Bouyssel, F., Tompkins, A. M., Wilson, D. R., Morille, Y., Haeffelin, M., O'Connor, E. J., Hogan, R. J., Illingworth, A. J., Donovan, D. P. and Baltink, H. K. (2010). Evaluation of operational model cloud representation using routine radar/lidar measurements. *J. Appl. Meteor. Clim*, **49**, 1971–1991.

Fu, Q. (1996). An accurate parameterization of the solar radiative properties of cirrus clouds. *J. Climate*, **9**, 2058–2082.

Fu, Q., Yang, P. and Sun, W. B. (1998). An accurate parametrization of the infrared radiative properties of cirrus clouds of climate models. *J. Climate*, **11**, 2223–2237.

Heymsfield, A. J. and Iaquinta, J. (2000). Cirrus crystal terminal velocities. *J. Atmos. Sci.*, **57**, 916–938.

Hogan, R. J., Behera, M. D., O'Connor, E. J. and Illingworth, A. J. (2007). Estimating the global distribution of supercooled liquid water clouds using spaceborne lidar. *Geophys. Res. Lett.*, **32**, DOI: 10.1029/2003GL018977.

Illingworth, A. J., Hogan, R. J. and coauthors (2007). Cloudnet - Continuous evaluation of cloud profiles in seven operational models using ground-based observations. *Bull. Amer. Meteor. Soc.*, **88**, 883–898.

Jakob, C. (2000). *The representation of cloud cover in atmospheric general circulation models*. Ph.D. thesis, University of Munich, Germany, available from ECMWF, Shinfield Park, Reading RG2 9AX, UK.

Jakob, C. and Klein, S. A. (2000). A parametrization of the effects of cloud and precipitation overlap for use in general circulation models. *Q. J. R. Meteorol. Soc.*, **126**, 2525–2544.

Kärcher, B. and Lohmann, U. (2002). A parameterization of cirrus cloud formation: Homogeneous freezing of supercooled aerosols. *J. Geophys. Res.*, **107**, DOI: 10.1029/2001JD000470.

Khvorostyanov, V. and Sassen, K. (1998). Cirrus cloud simulation using explicit microphysics and radiation. part ii: Microphysics, vapor and ice mass budgets, and optical and radiative properties. *J. Atmos. Sci.*, **55**, 1822–1845.

Koop, T., Luo, B. P., Tsias, A. and Peter, T. (2000). Water activity as the determinant for homogeneous ice nucleation in aqueous solutions. *Nature*, **406**, 611–614.

Lin, Y. L., Farley, R. D. and Orville, H. D. (1983). Bulk parameterization of the snow field in a cloud model. *J. Climate Appl. Meteorol.*, **22**, 1065–1092.

Lohmann, U. and Kärcher, B. (2002). First interactive simulations of cirrus cloud formed by homogeneous freezing in the ECHAM general circulation model. *J. Geophys. Res.*, **107**, 10.1029/2001JD000767.

Ma, H.-Y., Kohler, M., Li, J.-L. F., Farrara, J. D., Mechoso, C. R., Forbes, R. M. and Waliser, D. E. (2012). Evaluation of an ice cloud parametrization based on a dynamical-microphysical lifetime concept using CloudSat observations and the ERA-Interim reanalysis. *J. Geophys. Res.*, p. Accepted.

Meyers, M. P., DeMott, P. J. and Cotton, W. R. (1992). New primary ice nucleation parameterization in an explicit model. *J. Appl. Meteor.*, **31**, 708–721.

Pruppacher, H. R. and Klett, J. D. (1997). *The Microphysics of Clouds and Precipitation*. Kluwer Academic Publishers, pp. 954.

Ren, C. and Mackenzie, A. R. (2005). Cirrus parametrization and the role of ice nuclei. *Q. J. R. Meteorol. Soc.*, **131**, 1585–1605.

Rodwell, M. J., Haiden, T. and Richardson, D. S. (2011). Developments in precipitation verification. *ECMWF Newsletter No.*, **128**, 12–16.

Rodwell, M. J., Richardson, D. S., Hewson, T. D. and Haiden, T. (2010). A new equitable score suitable for verifying precipitation in numerical weather prediction. *Q. J. R. Meteorol. Soc.*, **136**, 1344–1363.

Rossow, W. B. and Schiffer, R. A. (1991). ISCCP cloud data products. *Bull. Amer. Meteor. Soc.*, **72**, 1–20.

Rossow, W. B., Walker, A., Beuschel, D. and Roiter, M. (1996). *International Satellite Cloud Climatology Project (ISCCP): Description of new cloud datasets*. "WMO/TD-737, World Climate Research Programme (ICSU and WMO), Geneva, Switzerland, 115 pp.".

Rotstayn, L., Ryan, B. and Katzfey, J. (2000). A scheme for calculation of the liquid fraction in mixed-phase stratiform clouds in large-scale models. *Mon. Wea. Rev.*, **128**(4), 1070–1088.

Sun, Z. (2001). Reply to comments by Greg M. McFarquhar on "Parametrization of effective sizes of cirrus-cloud particles and its verification against observations". *Q. J. R. Meteorol. Soc.*, **127**, 267–271.

Sun, Z. and Rikus, L. (1999). Parametrization of effective sizes of cirrus-cloud particles and its verification against observations. *Q. J. R. Meteorol. Soc.*, **125**, 3037–3055.

Sundqvist, H. (1978). A parameterization scheme for non-convective condensation including prediction of cloud water content. *Q. J. R. Meteorol. Soc.*, **104**, 677–690.

Tiedtke, M. (1993). Representation of clouds in large-scale models. *Mon. Wea. Rev.*, **121**, 3040–3061.

Tompkins, A. M., Gierens, K. and Rädel, G. (2007). Ice supersaturation in the ECMWF integrated forecast system. *Q. J. R. Meteorol. Soc.*, **133**, 53–63.

Wacker, U. and Seifert, A. (2001). Evolution of rain water profiles resulting from pure sedimentation: Spectral vs. parameterized description. *Atmos. Res.*, **58**, 19–39.

Waliser, D. E., Li, J.-L. F., L'Ecuyer, T. S. and Chen, W.-T. (2011). The impact of precipitating ice and snow on the radiation balance in global climate models. *Geophys. Res. Lett.*, **38**, DOI: 10.1029/2010GL046478.

Wielicki, B., Barkstrom, B. R., Harrison, E. F., Lee, R. B., Smith, G. L. and Cooper, J. E. (1996). Clouds and the Earth's Radiant Energy System (CERES): An Earth observing system experiment. *Bull. Amer. Meteor. Soc.*, **77**, 853–868.

Wielicki, B., Priestley, K., Minnis, P., Loeb, N., Kratz, D., Charlock, T., Doelling, D. and Young, D. (2006). CERES radiation budget accuracy overview. In *12th Conf. Atmospheric Radiation, Madison, WI, Amer. Meteor. Soc.*

Wilson, D. R. and Ballard, S. (1999). A microphysical based precipitation scheme for the UK Meteorological Office Unified Model. *Q. J. R. Meteorol. Soc.*, **125**, 1607–1636.